Building and Environment 272 (2025) 112672

Contents lists available at ScienceDirect

Building and Environment

journal homepage: www.elsevier.com/locate/buildenv

A novel methodology for the characterisation of airflow using infrared thermography and pressurisation test

Diego Tamayo-Alonso *, Alberto Meiss

GIR Arquitectura & Energía, Dpto. Construcciones Arquitectónicas I.T. y M.M.C.T.E., E.T.S Arquitectura, Universidad de Valladolid, Spain

ARTICLE INFO

Keywords:
Infiltration
Thermography
Air leakage
Pressurisation test
Building airtightness

ABSTRACT

Although buildings have reduced energy consumption in recent years, high levels remain, primarily due to HVAC systems. Air infiltration, which significantly impacts thermal comfort and energy efficiency, is critical. Pressurisation tests are widely used to assess the airtightness of building envelopes, but they do not identify the specific locations or shapes of air leaks.

In this context, combining thermography with pressurisation tools shows significant potential. Thermography enables the visualisation of temperature differences caused by air leaks, while pressurisation tests provide general information on a building's permeability. This approach offers a more comprehensive understanding of building airtightness. However, the methodology currently only provides a general quantitative indication of permeability and locates some leaks. While promising, further research is required to enhance the precision and ability to quantify and address air leakage issues.

This paper presents an experimental laboratory study to develop a methodology to characterise air infiltration. It uses a three-dimensional matrix placed near a controlled inlet, where cold air entering due to pressure differences alters the matrix's surface temperature. These changes are detected by infrared thermography, enabling accurate airflow characterisation. This approach effectively identifies and characterises air leakage from a single IR thermal image for each airflow condition, providing valuable data for decision-making.

1. Introduction

Since the 'Directive 93/76/EEC of 13 September 1993 to limit carbon dioxide emissions by improving energy efficiency', it has been repeatedly and unchanged stated that buildings consume about 40 % of the total energy in the European Union [1–7]. Similarly, the latest 'Directive (EU) 2024/1275 on the energy performance of buildings' states that buildings are responsible for 36 % of energy-related greenhouse gas emissions and that 75 % of buildings in the Union are still not energy efficient. The thermal conditioning of buildings accounts for the largest share of this energy consumption [8].

This scenario shows the need to redouble efforts to reduce the energy consumption of buildings from a global perspective, going beyond reducing the transmittance of the thermal envelope or increasing the efficiency of energy systems. Air infiltration in buildings significantly impacts their energy demand [9]. It is, therefore, essential to reduce this infiltration.

However, eliminating infiltration can often be complicated and costly. Therefore, it is essential to correctly identify infiltration and understand the significance of any one infiltration concerning the total. Previous methodologies have characterised infiltration using various methods such as active [10] and passive thermography and pressure testing [11]. This method approaches the problem of characterising infiltration from a three-dimensional point of view, making it possible to apply this concept to any infiltration. The problem lies in the number of thermographic images required to characterise a leak and, consequently, the time required, which makes it unlikely to be used in real cases.

This article presents a new methodology, tested in a laboratory, which approaches the characterisation of infiltrations from a three-dimensional point of view but improves the system for taking thermographic images. In this way, the methodology presented below makes it possible to characterise an infiltration with only one thermographic image. This reduces data acquisition and processing time by 96 % compared to the previous methodology.

2. State of the art

Infrared thermography (IRT) is a non-invasive method for

* Corresponding author.
E-mail address: diego.tamayo@uva.es (D. Tamayo-Alonso).

https://doi.org/10.1016/j.buildenv.2025.112672
Received 28 November 2024; Received in revised form 29 January 2025; Accepted 3 February 2025
Available online 4 February 2025

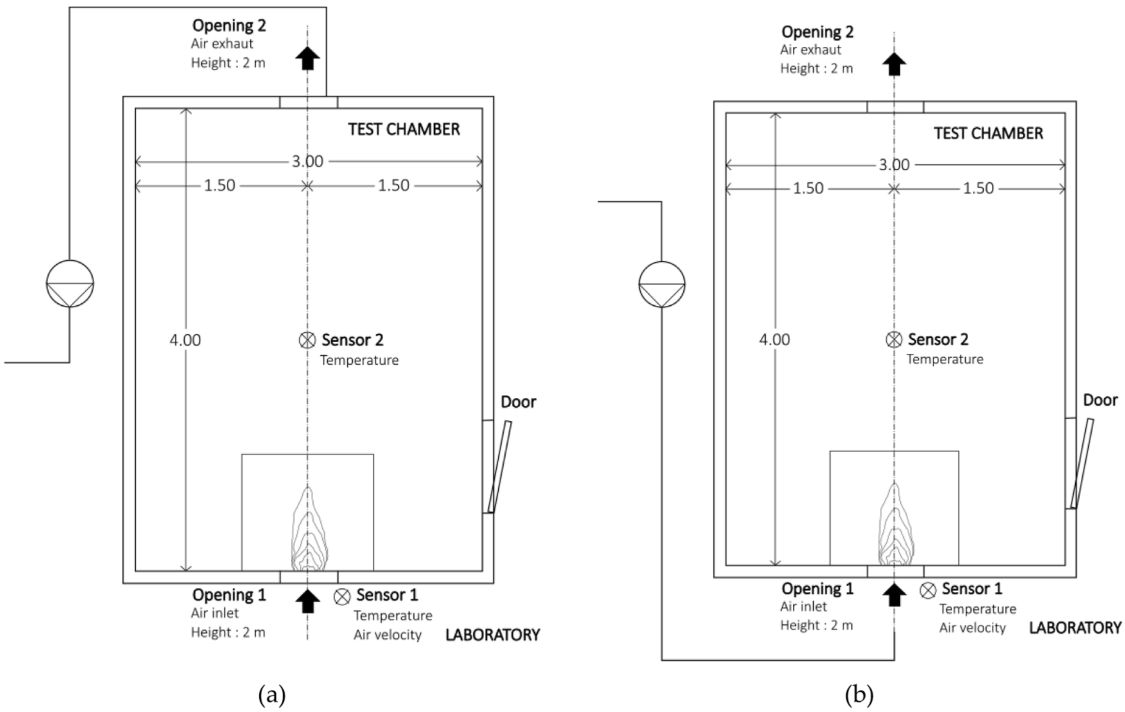

Fig. 1. (a) Sub-pressure test chamber configuration; (b) Over-pressure test chamber configuration.

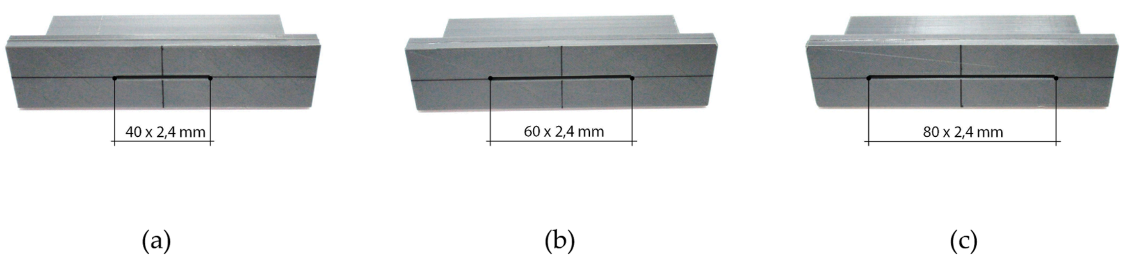

Fig. 2. Incoming airflow openings (a) A1. 40 mm x 2.4 mm (96 mm^2) (b) A2. 60 mm x 2.4 mm (144 mm^2) (c) A3. 80 mm x 2.4 mm (192 mm^2).

determining the surface temperature of objects without requiring physical contact between the measurement device and the object [12]. Recent advancements in thermographic technology have significantly expanded its applications, particularly in the energy analysis of buildings [13]. This growth in utility is evidenced by comprehensive reviews and studies that explore its role in assessing building envelope performance, identifying thermal anomalies, and improving energy efficiency.

Kirimtat and Krejcar (2018) conducted an extensive review of IRT applications in the study of building envelopes [10]. They identified air leakage as one of the most significant issues affecting the energy performance of buildings, noting that this issue is frequently addressed in the literature. This finding underscores the relevance of IRT in detecting and mitigating energy losses caused by envelope deficiencies.

Further advancing the field, a 2023 study by Gil-Docampo et al. explored the integration of IRT with unmanned aerial systems (UAS) for non-invasive detection of structural defects and comprehensive building envelope analysis [14]. The study used handheld and UAS-mounted thermal cameras to identify thermal anomalies such as thermal bridging, air leakage, and moisture intrusion. These findings highlight the versatility and precision of modern IRT techniques in diagnosing building envelope issues.

IRT has also been compared to traditional methods for building energy audits. Tardy critically evaluated IRT as an alternative to heat flow meters (HFM), emphasising its potential advantages and limitations when used alongside standard practices such as ISO 9869 [15]. This analysis contributes to understanding how IRT complements or

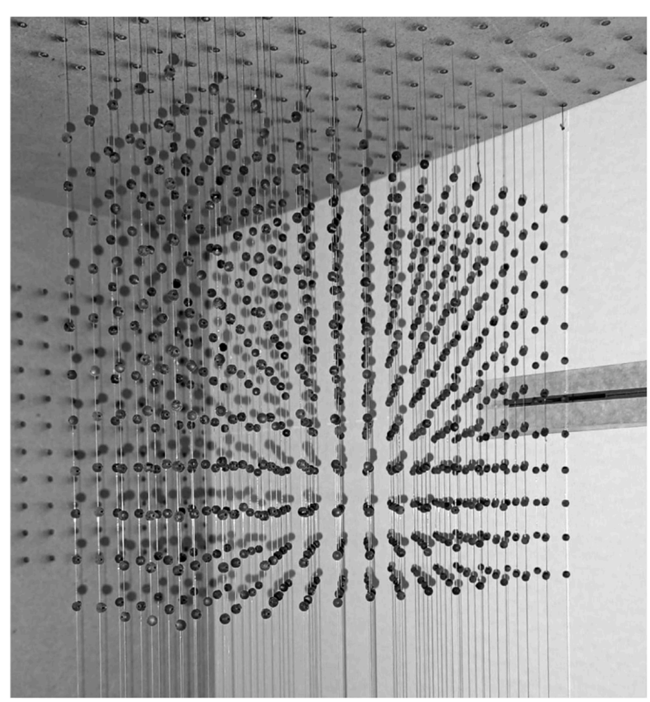

Fig. 3. Three-dimensional matrix.

(a) (b)

Fig. 4. (a) Laser levelling of the matrix (b) Set-up of the experiment.

challenges established methodologies in building performance evaluation.

Building airtightness, a critical factor in energy performance, has also been extensively reviewed. Poza highlighted the growing importance of airtightness, providing a comprehensive overview of significant airtightness databases and testing setups across Europe and North America [16]. Various methodologies have been developed to quantify air infiltration, ranging from mathematical models to experimental and simulation-based approaches. Notable examples include the development of a quadratic relationship to define air inlet parameters [17] and foundational work on infiltration parameterisation by Murakami and Kato [18]

Zheng et al. reviewed methods for measuring building airtightness, highlighting its importance as a key indicator of construction quality and envelope integrity. The impact of external factors, such as wind, on airtightness measurements has been examined. Carrié and Mélois developed a physical model to assess the impact of unsteady wind on pressurisation test results, providing valuable insights into uncertainties that current standards often overlook [19].

Thermography's role in detecting air leakage has been extensively demonstrated in literature. Mahmoodzadeh et al. [20] showed that temperature differences on building surfaces can effectively identify leakage points. Similarly, Barreira et al. [21] and Avdelidis and Kauppinen [22] documented IRT's ability to pinpoint leakage locations around windows, doors, and service penetrations. Recent advancements include the combination of thermography with pressurisation techniques. Kölsch et al. [23] demonstrated the effectiveness of using thermograms before and after thermal excitation and mathematical post-processing to locate infiltrations around windows. Hurel et al. [24]used thermography and PIV methods to characterise the air inlets and outlets in wall assemblies. The PIV method is very interesting to characterise the airflow of infiltration in a laboratory, but it is not easy to

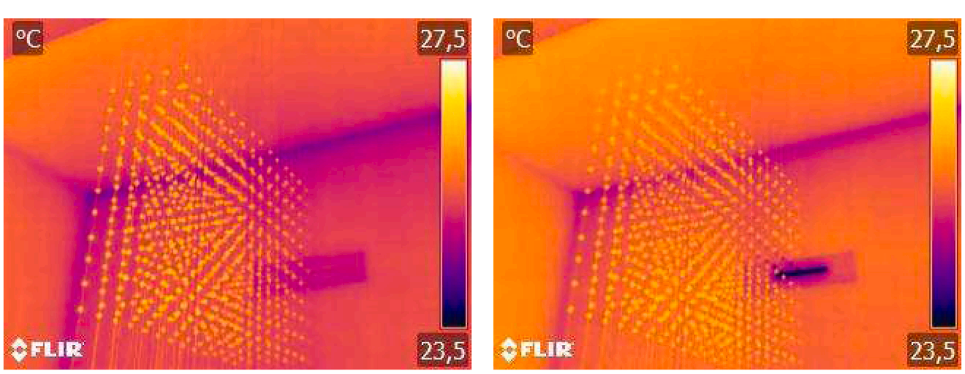

(a) (b)

Fig. 5. (a) Pre-excitation thermography (b) Post-excitation thermography.

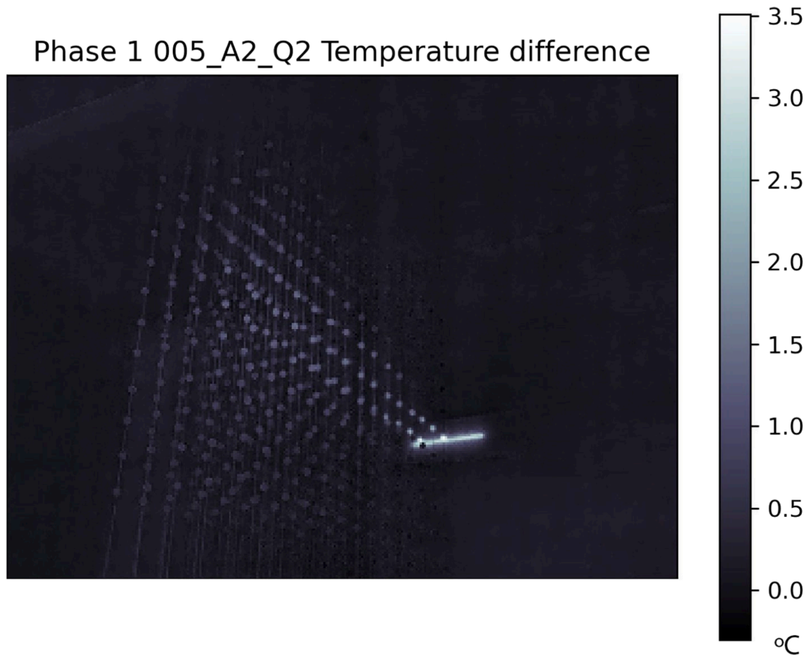

Fig. 6. Imagen obtained of the subtracting temperatures.

Table 1
Test flow rates.

Test airflow			
	Q1	Q2	Q3
A1	0.5 m^3/h	2.3 m^3/h	3.7 m^3/h
A2	0.8 m^3/h	3.4 m^3/h	5.0 m^3/h
A3	1.1 m^3/h	4.2 m^3/h	5.6 m^3/h

implement this method in actual cases.

Beyond two-dimensional analyses, research has explored three-dimensional characterisations of airflow through controlled openings. Gil-Valverde et al. developed a methodology that minimises the Coanda effect [11], an issue noted in previous studies [25,26]. This innovative approach involves capturing thermograms across multiple cutting planes and synthesising them into a three-dimensional matrix, offering a

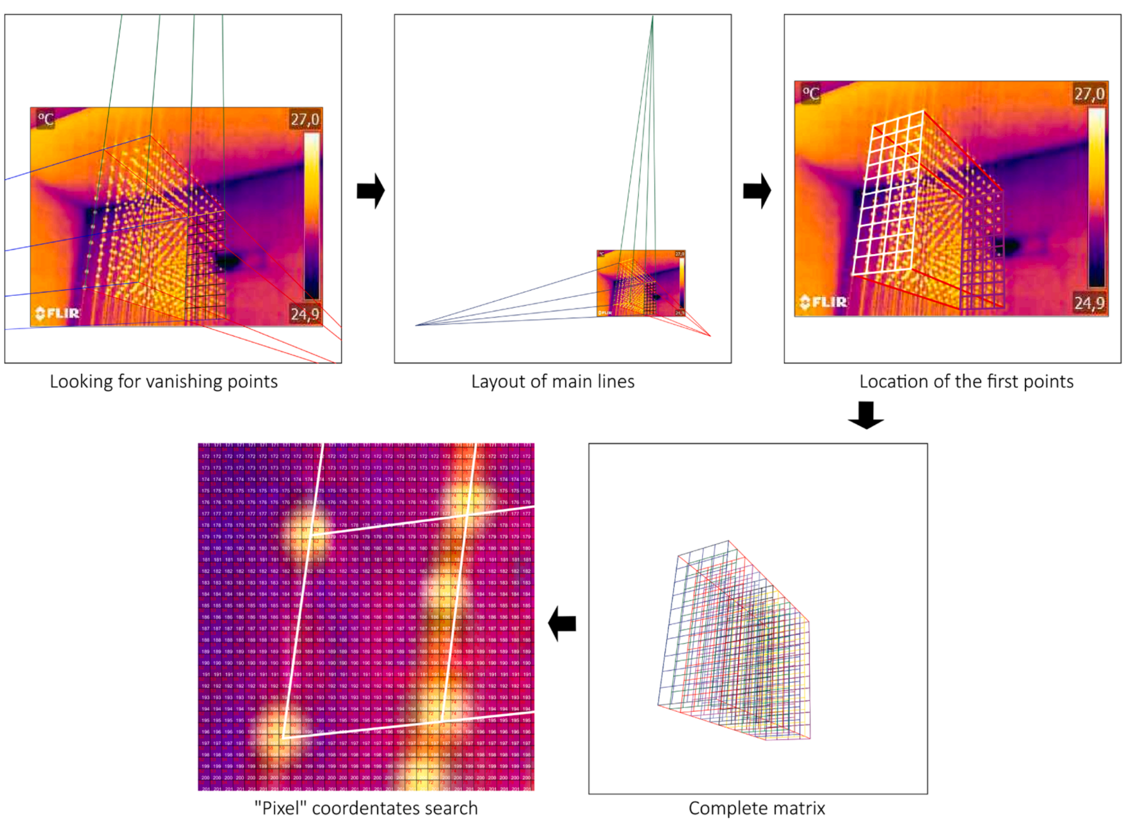

Fig. 7. Procedure to obtain the pixel of each sphere.

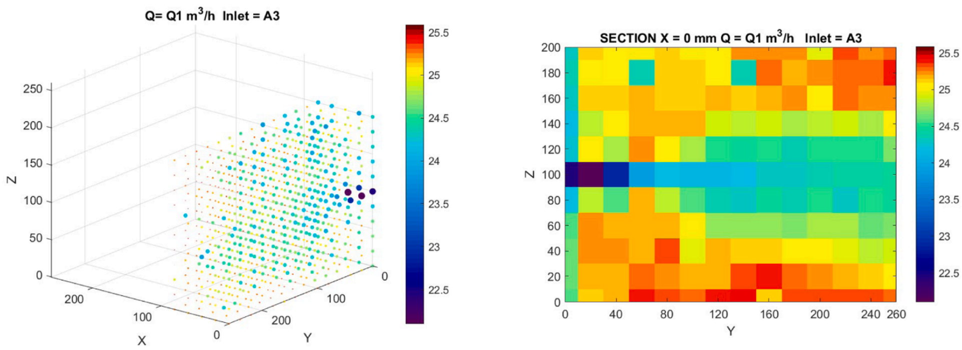

(a) (b)

Fig. 8. (a) Tri-dimensional matrix of temperatures; (b) Slice for $X = 0$ mm.

more detailed representation of infiltration patterns. This methodology takes much time to capture and post-process the data. Every cutting plane needs to change the plane manually, wait for stabilised temperatures for around 15 min, turn on the fan, wait again for 10 min and take the thermography. This process was repeated for the eleven cutting planes to get all the data for building the three-dimensional matrix. Finally, getting the data takes around five or six hours. Also, every thermography must be post-processed, which takes around three hours

Table 2
Data collected in the tests.

Test	Opening	Config Chamber	ΔPre (Pa)	Q (m^3/h)	Area (mm^2)	V_{out} (m/s)	T_{int} (°C)	T_{ext} (°C)	ΔT (°C)
001	A1	Sub-pressure	−5	1.4	96	3.9	26.1	20.9	−5.2
002	A1	Sub-pressure	−5	1.2	96	3.5	26.5	20.9	−5.6
003	A1	Sub-pressure	−33	2.6	96	7.4	26.2	21.0	−5.2
004	A1	Sub-pressure	−33	2.4	96	7.0	26.3	21.0	−5.3
005	A1	Sub-pressure	−89	3.9	96	11.3	26.2	21.0	−5.2
006	A1	Sub-pressure	−88	3.8	96	10.9	26.0	20.9	−5.1
007	A2	Sub-pressure	−1	2.2	144	4.1	26.0	20.5	−5.5
008	A2	Sub-pressure	−2	2.1	144	4.0	25.4	20.2	−5.2
009	A2	Sub-pressure	−5	1.3	144	2.47	25.7	20.7	−5.1
010	A2	Sub-pressure	−35	3.1	144	5.9	25.3	20.3	−5.0
011	A2	Sub-pressure	−34	4.1	144	7.8	25.8	20.5	−5.3
012	A2	Sub-pressure	−34	3.6	144	6.9	25.7	20.7	−5.0
013	A2	Sub-pressure	−89	5.2	144	9.9	25.4	20.3	−5.2
014	A2	Sub-pressure	−90	5.2	144	9.9	25.6	20.5	−5.1
015	A2	Sub-pressure	−89	5.2	144	9.9	26.0	20.7	−5.3
016	A3	Sub-pressure	−5	2.7	192	3.9	24.9	19.7	−5.3
017	A3	Sub-pressure	−5	3.1	192	4.4	25.0	19.9	−5.1
018	A3	Sub-pressure	−34	4.7	192	6.8	24.6	19.6	−5.1
019	A3	Sub-pressure	−33	4.7	192	6.8	25.1	19.8	−5.3
020	A3	Sub-pressure	−90	5.7	192	8.2	24.7	19.5	−5.2
021	A3	Sub-pressure	−89	5.7	192	8.2	25.3	19.8	−5.5
022	A1	Sub-pressure	−5	0.5	96	1.4	24.4	19.1	−5.3
023	A1	Sub-pressure	−34	2.3	96	6.6	24.5	19.2	−5.2
024	A1	Sub-pressure	−91	3.7	96	10.7	24.5	19.3	−5.2
025	A2	Sub-pressure	−5	0.9	144	1.6	25.5	20.1	−5.4
026	A2	Sub-pressure	−34	3.5	144	6.6	25.3	20.2	−5.1
027	A2	Sub-pressure	−89	5.1	144	9.7	25.2	20.2	−5.1
028	A3	Sub-pressure	−4	1.1	192	1.5	25.3	20.3	−5.1
029	A3	Sub-pressure	−33	4.2	192	6.1	25.4	20.4	−5.0
030	A3	Sub-pressure	−89	5.6	192	8.0	25.5	20.3	−5.2
031	A1	Over-pressure	0	0.5	96	1.5	24.7	19.4	−5.4
032	A1	Over-pressure	0	3.5	96	10.1	24.5	19.5	−5.1
033	A1	Over-pressure	0	6.5	96	18.8	24.6	19.3	−5.3
034	A1	Over-pressure	0	0.5	96	1.5	24.7	19.5	−5.2
035	A1	Over-pressure	0	3.5	96	10.0	24.8	19.6	−5.2
036	A1	Over-pressure	0	6.6	96	18.9	25.1	19.6	−5.4
037	A2	Over-pressure	0	0.5	144	1.0	24.7	19.7	−5.0
038	A2	Over-pressure	0	3.6	144	6.9	25.0	19.9	−5.1
039	A2	Over-pressure	0	6.5	144	12.5	25.2	19.8	−5.4
040	A2	Over-pressure	0	0.5	144	1.0	25.1	19.9	−5.2
041	A2	Over-pressure	0	3.5	144	6.8	25.0	20.0	−5.0
042	A2	Over-pressure	0	6.5	144	12.5	25.3	19.9	−5.4
043	A3	Over-pressure	0	0.5	192	0.7	25.7	20.4	−5.3
044	A3	Over-pressure	0	3.5	192	5.0	25.7	20.6	−5.2
045	A3	Over-pressure	0	6.6	192	9.5	25.9	20.4	−5.5
046	A3	Over-pressure	0	0.7	192	0.9	25.7	20.5	−5.2
047	A3	Over-pressure	0	3.6	192	5.1	25.8	20.6	−5.2
048	A3	Over-pressure	0	6.6	192	9.4	26.0	20.6	−5.4

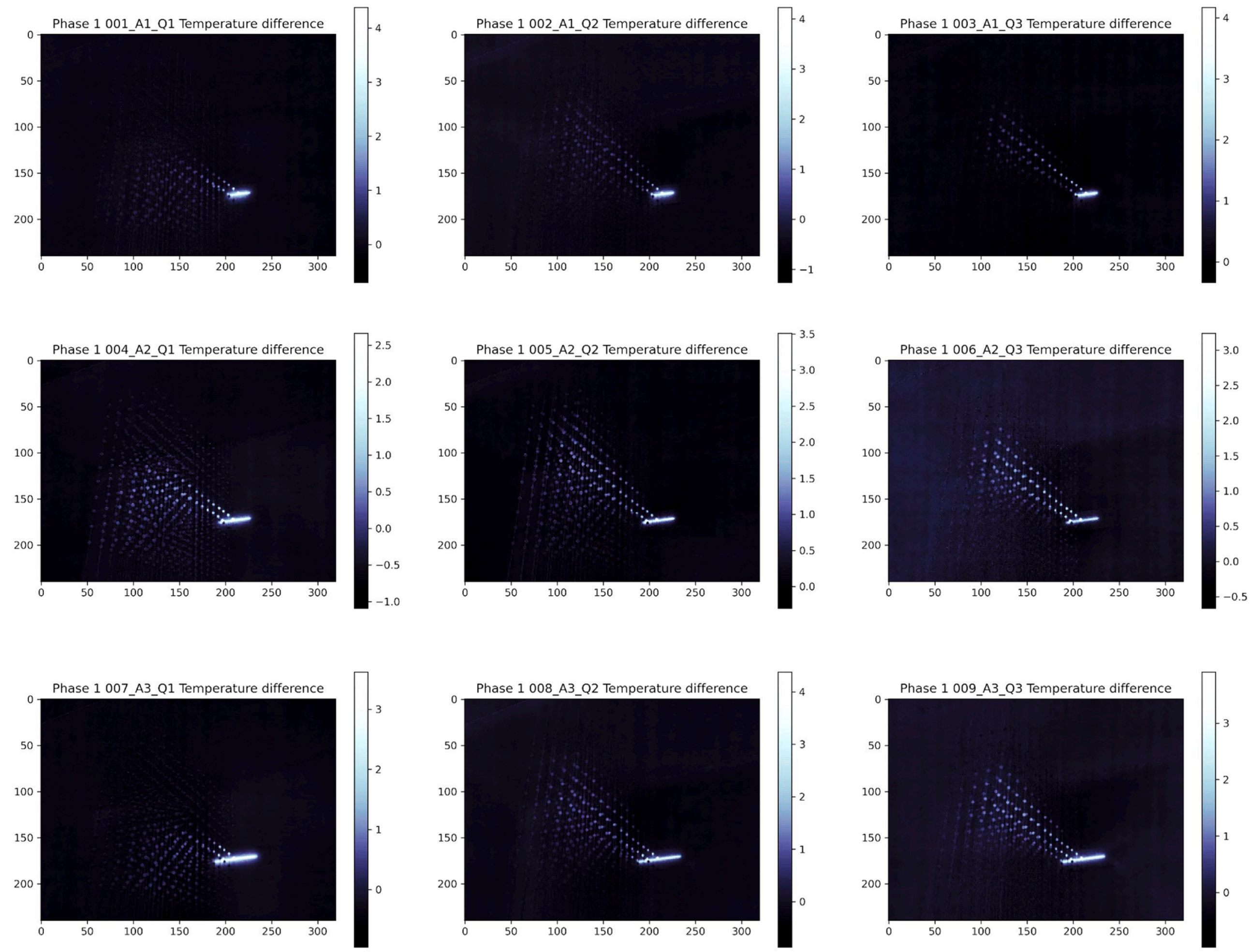

Fig. 9. Comparison of the nine tests in phase 1.

more. If we add the time to obtain the data plus the post-processing time, we would need between 8 and 9 h to obtain a three-dimensional matrix of an airflow. This makes the procedure unfeasible to implement in a real case.

3. Materials and methods

The experimental phase was divided into two parts. The first corresponds to a qualitative phase. It involved conducting thermography before and after excitation and obtaining an image with the temperature difference. This first phase allows us to see the airflow and observe if it follows a logical pattern with the opening or flow rate change.

The temperature was extracted from the measurement points in the second phase and transposed to a digital model. This model makes it possible to use any point or set of these points, for example, to create slices along any axis. This phase is more quantitative and less visual but finally gives us more information than the first phase. The final objective is to obtain the characterisation of the airflow through an opening, in this case, controlled.

3.1. Equipment and laboratory experimental set-up

Both phases were developed in a controlled test chamber in the Ventilation Laboratory HS3 (University of Valladolid). The test chamber measures 3.0 m x 4.0 m x 2.5 m (height) and has openings that can be configured as inlet, outlet, or closed (Fig. 1).

The controlled airflow openings have been made using additive 3D printing and hot melt polylactide plastic (PLA) as the base material. The unique change between the three openings is the width inlet, which guarantees the precision of the dimensions between the pieces. The experiment has been involved in testing three different incoming airflow openings with varying inlet areas. The dimensions were adjusted by increasing the width while keeping the height constant at 2.4 mm in each case. (Fig. 2)

Airflow rate through the test chamber and inlet and outlet temperatures have been monitored by a multisensory data logger Delphin Loggito. High-precision TSIC 501F sensors (accuracy $\pm$0.1 K) were used to measure temperatures at specified points in the test chamber configuration, and IST FS5 sensors (accuracy $\leq$ 3 %) were used to measure airflow.

The thermographic images were taken using an IR camera, Flir E75, with a resolution of 320$\times$240. The measurement device was a three-dimensional matrix of spheres spaced 20 mm apart. (see Fig. 3). The spheres were made in the laboratory using black printing resin as the material, which has an emissivity of ε=0.95. The finish of this material is rather matt, thus avoiding reflections that distort the measurements.

The three-dimensional sphere matrix was mounted in a wooden box opened on two sides and placed on the wall of another wooden structure. The set was laser-levelled to ensure the correct positioning of the matrix (see Fig. 4).

3.2. Test chamber configuration

The test chamber's inlet and outlet were positioned opposite each

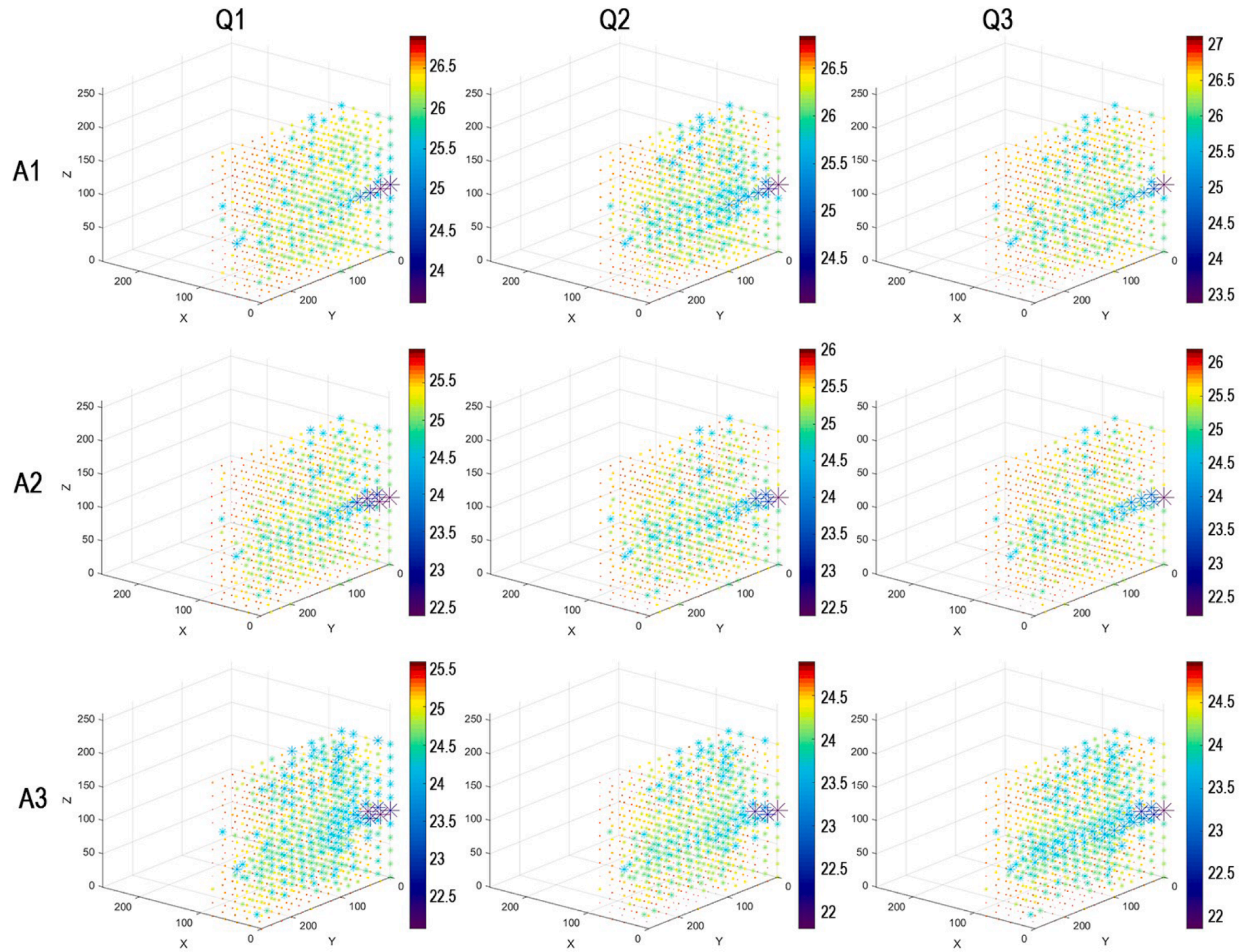

Fig. 10. Comparison of 3D graphics of the nine combinations of flow and opening in phase 2.

other. Its sealed construction ensures balanced airflow perpendicular to the wall surface where the incoming air openings were situated.

In order to create a negative pressure in the chamber, a fan was placed at the opening 2 of the chamber and exhausts air. This sub-pressure forced the airflow through the opening we had generated. The airflow was regulated by connecting the fan to a frequency shifter, thus controlling the chamber sub-pressure and, consequently, the air inlet flow. As a result, this configuration created a negative pressure inside the test chamber, forcing air through the inlet. On the other hand, to create a positive pressure in the chamber, the fan was placed at the opening 1 and insufflated air into the chamber. In this case, the direct air supply was measured. (see Fig. 1)

In order to ensure the maintenance of a constant interior temperature, the test chamber was equipped with an underfloor radiant heating system, which minimises the convection effect that other heating systems could generate. This system was controlled automatically by the logger, ensuring a consistent five-degree Celsius temperature difference between the interior and exterior of the chamber. The incoming air was sourced directly from the laboratory. Maintaining this constant temperature contrast created a thermal environment within the test chamber, enhancing the reproducibility of obtained infrared images. To minimise interference from heat radiation emitted by the heating system, a Lambert radiator has been positioned between the area under study and the floor.

3.3. Development of the test

The experiment's first phase consisted of capturing an IR thermographic image before and after the excitation (Fig. 5). The second IR thermographic image was taken when the airflow was stabilised, and a constant thermal path was obtained.

The stabilisation time was determined by an empirical method after studying the thermal path performance in different time ranges. The surface temperature was studied for ten minutes by recording a thermographic video. These essays observed that the temperatures were stabilised in an interval between two and three minutes. Based on these results, it was decided to take the second thermography five minutes after the start of the fan.

Once the two thermographs have been obtained, the next step is to subtract the temperatures pixel by pixel to obtain the points that have changed in temperature after the cold air has passed through the beads (Fig. 6). At this point, the point of view needed not to change.

Nine tests were performed, one for each combination of fan speed and opening (Table 1). The flow rate varied between openings at the same fan frequency due to the change in pressure drop caused by the opening.

These results were used to validate the correct airflow behaviour. The balls hardly interfered with the airflow and provided an excellent visual characterisation of the airflow.

The second phase of the experiment was to take an IR thermographic image once the temperatures were stabilised, with the same waiting time as in the previous phase. The temperatures were extracted from

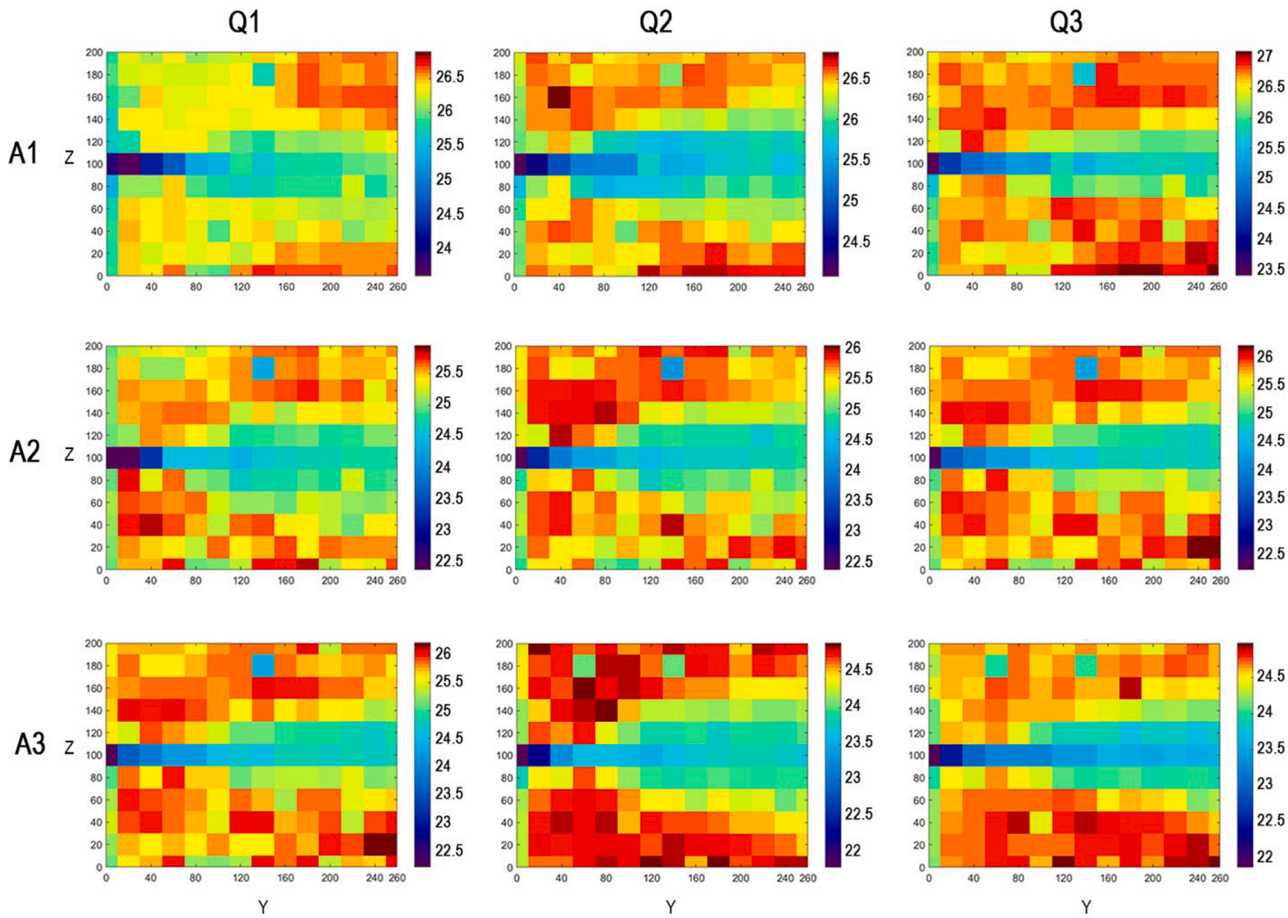

Fig. 11. Comparison of the perpendicular vertical plan of dimension $X = 0$ of the nine combinations of flow and opening in phase 2.

Table 3
Pairs of compared tests.

Test	Opening	Config Chamber	ΔPre (Pa)	Q (m^3/h)	Area (mm^2)	V_{out} (m/s)	T_{int} (°C)	T_{ext} (°C)	ΔT (°C)
031	A1	Over-pressure	0	0.5	96	1.5	24.7	19.4	−5.4
034	A1	Over-pressure	0	0.5	96	1.5	24.7	19.5	−5.2
038	A2	Over-pressure	0	3.6	144	6.9	25.0	19.9	−5.1
041	A2	Over-pressure	0	3.5	144	6.8	25.0	20.0	−5.0
045	A3	Over-pressure	0	6.6	192	9.5	25.9	20.4	−5.5
048	A3	Over-pressure	0	6.6	192	9.4	26.0	20.6	−5.4

each sphere to form a 3D array. The process can be divided into four stages.

The first stage was to identify the "pixel" for each sphere through geometry. This process was done manually but could be automated in the future. The locations of all the points were plotted, and a table was created with the absolute coordinates of the points and their "pixel" (Fig. 7).

The points of the matrix that were hidden behind others were carefully examined. The point of view was previously studied to minimise this problem as much as possible. It was observed that 29 out of 770 points were hidden, which is 3.7 %. Although an error of 3.7 % of the points could be considered negligible, analysis of the points showed that most of them were outside the airflow we were observing.

The second stage was to map the points with their corresponding temperatures on the thermography. This mapping was valid as long as the test elements' location, sphere matrix, and camera position and viewpoint were not changed. To maintain this throughout the tests, all the elements were marked with their position relative to the base. If an element had to be moved, it was perfectly repositioned in its original position.

In the third stage, the temperatures of each ball were extracted using an algorithm programmed in MATLAB. Together with the absolute coordinates of each point in millimetres, a table was created with the location of each sphere and its temperature.

Finally, a three-dimensional graph is obtained, displaying the temperature of each sphere. The graph's points vary in size and colour based on temperature to better illustrate the airflow. In the same way, using another algorithm, each matrix plane could be extracted according to the one that is more representative of the flow. In the case under study, this plane corresponded to the ZY axes, the vertical plane perpendicular to the opening (Fig. 8).

In this second phase, several essays were done with different configurations. The configuration tests were collected in Table 2. Within these tests, tests 1 to 30 were carried out with the test chamber at negative pressure and others, numbers 31 to 48, at positive pressure. In the case of the overpressure tests, in order to better control the flow rate, it was decided not to keep the fan speed fixed but to keep the flow rates stable so that the tests could be carried out over the flow rate.

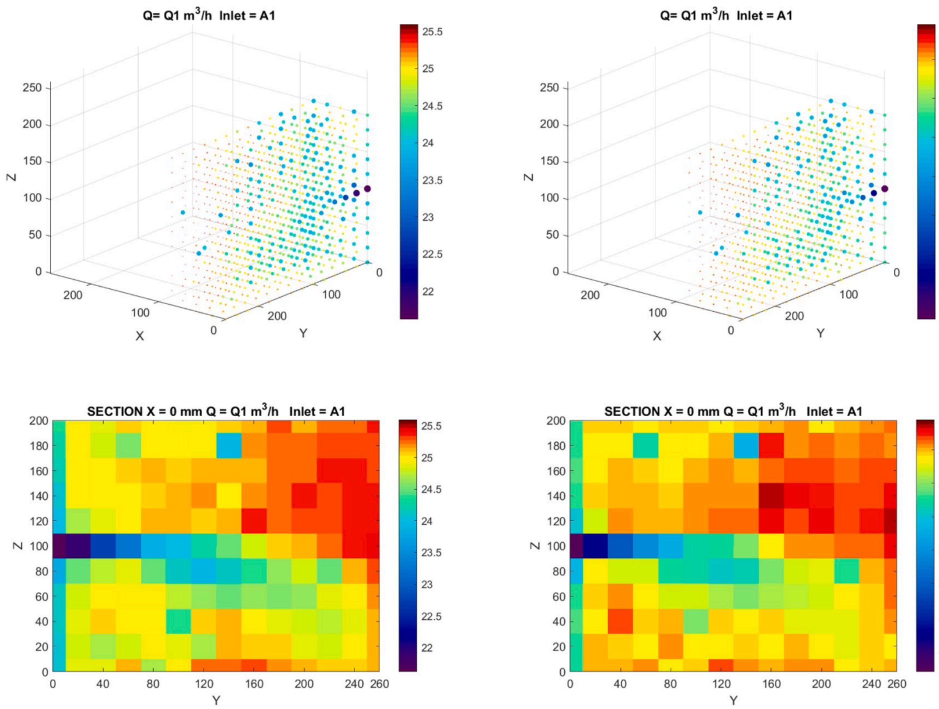

(a) (b)

Fig. 12. (a) 3D graph and section $X = 0$ for test 031; (b) 3D graph and section $X = 0$ for test 034.

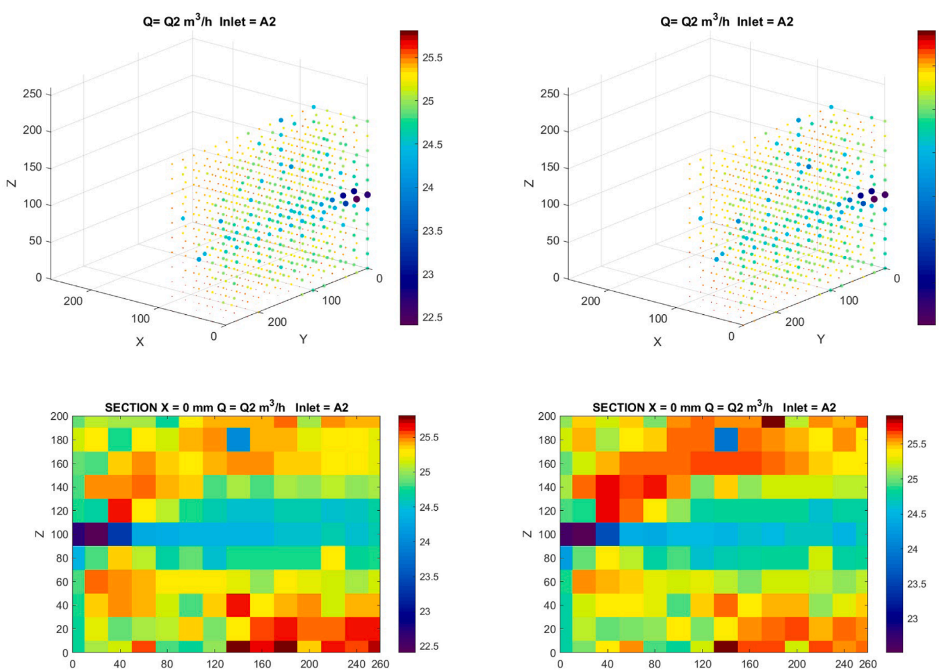

(a) (b)

Fig. 13. (a) 3D graph and section $X = 0$ for test 038; (b) 3D graph and section $X = 0$ for test 041.

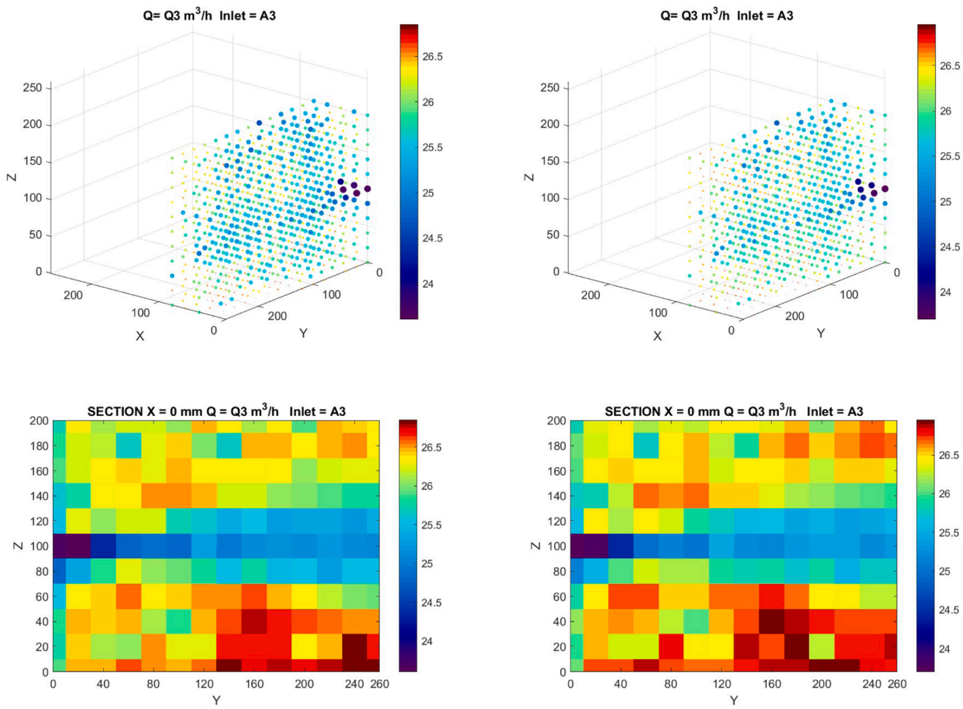

(a) (b)

Fig. 14. (a) 3D graph and section $X = 0$ for test 031; (b) 3D graph and section $X = 0$ for test 034.

Table 4
Compared tests with the same flow rate.

Test	Opening	Config Chamber	ΔPre (Pa)	Q (m^3/h)	Area (mm^2)	V_{out} (m/s)	T_{int} (°C)	T_{ext} (°C)	ΔT (°C)
001	A1	Sub-pressure	−5	1.4	96	3.9	26.1	20.9	−5.2
007	A2	Sub-pressure	−1	2.2	144	4.2	26.0	20.5	−5.5
016	A3	Sub-pressure	−5	2.7	192	3.9	24.9	19.7	−5.3
006	A1	Sub-pressure	−88	3.8	96	10.9	26.0	20.9	−5.1
013	A2	Sub-pressure	−89	5.2	144	9.2	25.4	20.3	−5.2
020	A3	Sub-pressure	−90	5.7	192	8.2	24.7	19.5	−5.2

4. Results

The first phase provides an excellent qualitative visual characterisation of the airflow. This test allowed us to perfectly observe the trajectory, shape, and actual dispersion of the airflow paths corresponding to the different opening and airflow combinations. The following image (Fig. 9) compares the nine opening and fan speed combinations with the test chamber in depression mode.

In the second phase, the airflow was qualitatively compared with the temperature data. Now, only the temperatures of the spheres were taken. The 3D matrix obtained allows us to extract only one plane. The vertical perpendicular plane is the most representative of this type of opening. The following figures (Figs. 10 and 11) show a comparative sample of the nine flow and opening combinations from the 3D plots and the vertical perpendicular plane of dimension $X = 0$.

5. Analysis and discussion

Firstly, we compare the tests carried out under the same flow rate and opening conditions. For this comparison, we use the tests done under overpressure because these are the tests performed under equal flow rates. The compared test conditions are shown in Table 3.

Figs. 12–14 show that the airflow behaves uniformly under the same flow rate conditions, inlet, and thermal differential. This ensures system consistency and uniformity of results.

In the following section, we can analyse how the airflow behaviour changes with different openings. For this purpose, we can compare tests 001, 007, and 016, which were carried out with a Q1 flow rate, and tests 006, 013, and 020, which were carried out with a Q3 flow rate (Table 4).

It is possible to observe the behaviour of the air as we increase the inlet. We notice that at $X = 20$, we can see how the air impacts this area. Furthermore, if we compare Fig. 15a and Fig. 15d, we can see the difference in air outlet velocity due to the increased flow rate in Fig. 15d, which affects the airflow at $X = 20$, unlike in Fig. 15a.

However, Fig. 16 shows the change that occurs with increasing flow rate at the same aperture.

Fig. 16 shows how the airflow takes on a more horizontal and elongated component as we increase the flow rate. At a low flow rate (Q1), regardless of the inlet, the cold and denser air begins to descend earlier than the more significant flow rates (Q2 and Q3). However, as the velocity increases, this descent disappears in the measurement zone. In addition, between the flow Q2 and Q3 flows, the airflow dispersion decreases, and the cold air path narrows.

All these analyses, carried out from different perspectives, show that the data obtained with this method are robust and consistent. This is imperative to ensure reliability, as it is a prerequisite for data accuracy. This robustness of data makes it possible to characterise the airflow through an opening effectively. This characterisation is important for

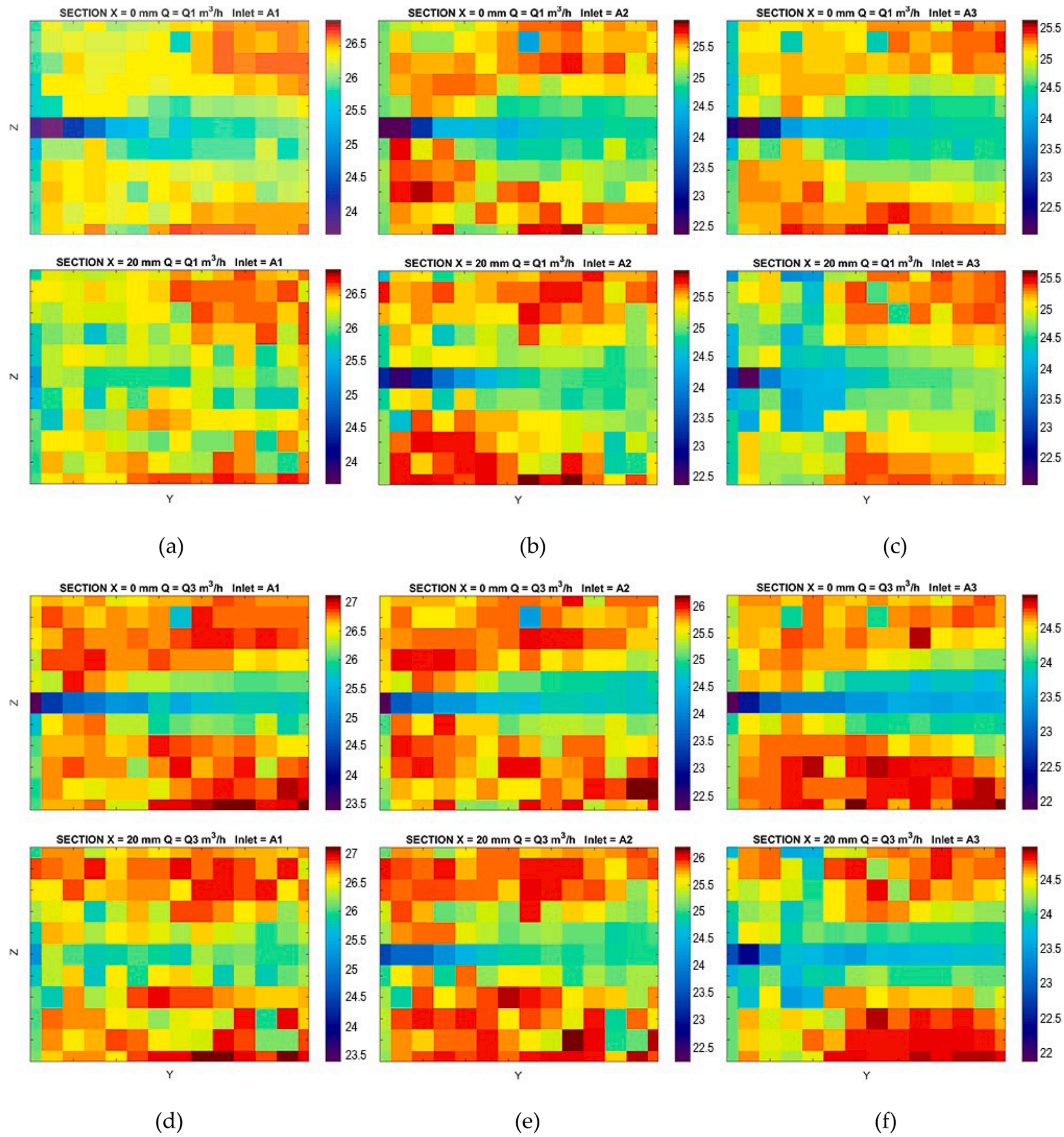

Fig. 15. (a) Section $X = 0$ and section $X = 20$ for test 001; (b) Section $X = 0$ and section $X = 20$ for test 007; (c) Section $X = 0$ and section $X = 20$ for test 016; (d) Section $X = 0$ and section $X = 20$ for test 006; (e) Section $X = 0$ and section $X = 20$ for test 013; (f) Section $X = 0$ and section $X = 20$ for test 020.

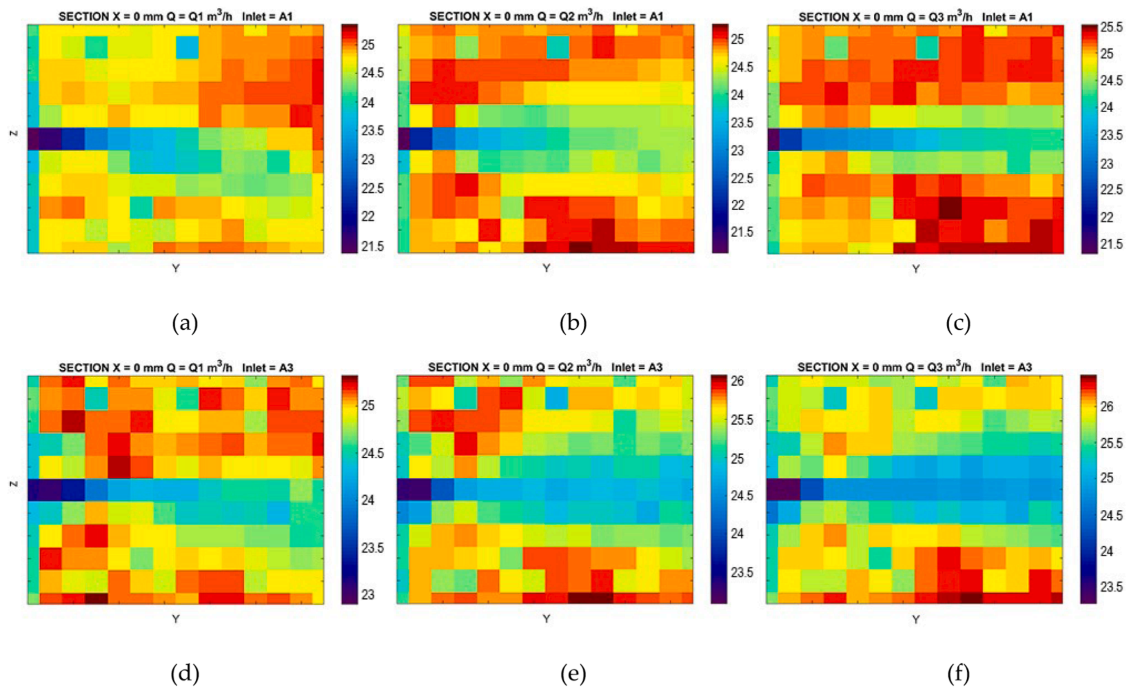

Fig. 16. (a) Section $X = 0$ for test 022; (b) Section $X = 0$ for test 023; (c) Section $X = 0$ for test 024; (d) Section $X = 0$ for test 028; (e) Section $X = 0$ for test 029; (f) Section $X = 0$ for test 030.

understanding airflow behaviour under different conditions, and it has significant applications in many fields of research or practical use.

6. Conclusion

This paper presents an improved method for characterising airflows through controlled air inlets. Unlike previous methods, which required extensive data collection, this technique only needs a single IR thermal image for each airflow condition. A single thermographic image provides a "steady-stage" airflow image. It should also be noted that we have worked with a slight thermal gradient of 5 °C, obtaining conclusive results. The results obtained are expected to be better with higher temperature gradients. All these methodological simplifications will allow the future use of the system in real cases.

In addition, using a single thermal image eliminates uncertainties related to pressure and temperature fluctuations during the measurement, as well as variations in camera location due to limited battery life.

In the future, machine learning can infer the flow rate from the thermographic IR, the inlet temperature, and the outlet temperature.

This method of airflow characterisation opens up new possibilities in several research topics, such as leakage quantification, *in situ* assessment of heat recovery systems or vents' operating regimes, and validation of CFD numerical studies.

Funding

This research has received external funding through the research project "Ventilación inteligente para una Calidad del aire interior saludable en las viviendas españolas (ES-VEN)", PID2022–142104OB-I00, funded by the Ministry of Science and Innovation of the Government of Spain.

CRediT authorship contribution statement

Diego Tamayo-Alonso: Writing – original draft, Visualization, Software, Project administration, Methodology, Investigation, Data curation, Conceptualization. **Alberto Meiss:** Writing – review & editing, Validation, Supervision, Project administration, Funding acquisition.

Declaration of competing interest

The authors declare the following financial interests/personal relationships which may be considered as potential competing interests:

Alberto Meiss reports financial support was provided by Ministry of Science and Innovation of the Government of Spain. If there are other authors, they declare that they have no known competing financial interests or personal relationships that could have appeared to influence the work reported in this paper.

Data availability

Data will be made available on request.

References

[1] Directive 93/76/EEC, (1993). https://eur-lex.europa.eu/eli/dir/1993/76/oj.
[2] Directive 2002/91/EC, (2002). https://eur-lex.europa.eu/eli/dir/2002/91/oj (accessed November 22, 2024).
[3] Directive 2010/31/EU, (2010). https://eur-lex.europa.eu/legal-content/EN/TXT/?uri=CELEX%3A32010L0031&qid=1732264646887 (accessed November 22, 2024).
[4] Directive 2012/27/EU, (2012). https://eur-lex.europa.eu/legal-content/EN/TXT/?uri=CELEX%3A32012L0027&qid=1732264698436 (accessed November 22, 2024).
[5] Directive (EU) 2018/844, (2018). https://eur-lex.europa.eu/eli/dir/2018/844/oj (accessed November 22, 2024).
[6] Directive (EU) 2023/1791, (2023). https://eur-lex.europa.eu/legal-content/EN/TXT/?uri=CELEX%3A32023L1791&qid=1732264749520 (accessed November 22, 2024).
[7] Directive (EU) 2024/1275, (2024). https://eur-lex.europa.eu/legal-content/EN/TXT/?uri=CELEX%3A32024L1275&qid=1732264800081 (accessed November 22, 2024).
[8] UN Environment Programme, Global Status Report for Building and Construction - towards a zero-emissions, efficient and resilient buildings and construction sector., 2019.
[9] J. Feijó-Muñoz, C. Pardal, V. Echarri, J. Fernández-Agüera, R. Assiego de Larriva, M. Montesdeoca Calderín, I. Poza-Casado, M.Á. Padilla-Marcos, A. Meiss, Energy impact of the air infiltration in residential buildings in the mediterranean area of Spain and the Canary islands, Energy Build. (2019), https://doi.org/10.1016/j.enbuild.2019.02.023.

[10] A. Kirimtat, O. Krejcar, A review of infrared thermography for the investigation of building envelopes: advances and prospects, Energy Build. 176 (2018) 390–406, https://doi.org/10.1016/j.enbuild.2018.07.052.
[11] R. Gil-Valverde, D. Tamayo-Alonso, A. Royuela-del-Val, I. Poza-Casado, A. Meiss, M.Á. Padilla-Marcos, Three-dimensional characterization of air infiltration using infrared thermography, Energy Build. 233 (2021) 110656, https://doi.org/10.1016/J.ENBUILD.2020.110656.
[12] R. Usamentiaga, P. Venegas, J. Guerediaga, L. Vega, J. Molleda, F. Bulnes, Infrared thermography for temperature measurement and non-destructive testing, Sensors 14 (2014) 12305–12348, https://doi.org/10.3390/s140712305.
[13] E. Lucchi, Applications of the infrared thermography in the energy audit of buildings: a review, Renew. Sustain. Energy Rev. 82 (2018) 3077–3090, https://doi.org/10.1016/j.rser.2017.10.031.
[14] M. Gil-Docampo, J.O. Sanz, I.C. Guerrero, M.F. Cabanas, UAS IR-thermograms processing and photogrammetry of thermal images for the inspection of building envelopes, Appl. Sci. (2023) 13, https://doi.org/10.3390/app13063948 (Switzerland).
[15] F. Tardy, A review of the use of infrared thermography in building envelope thermal property characterization studies, J. Build. Eng. 75 (2023), https://doi.org/10.1016/j.jobe.2023.106918.
[16] I. Poza-Casado, V.E.M. Cardoso, R.M.S.F. Almeida, A. Meiss, N.M.M. Ramos, M.Á. Padilla-Marcos, Residential buildings airtightness frameworks: a review on the main databases and setups in Europe and North America, Build. Environ. 183 (2020), https://doi.org/10.1016/j.buildenv.2020.107221.
[17] P.H. Baker, S. Sharples, I.C. Ward, Air flow through cracks, Build. Environ. (1987), https://doi.org/10.1016/0360-1323(87)90022-9.
[18] S. Murakami, S. Kato, Numerical and experimental study on room airflow-3-D predictions using the k-ε{lunate} turbulence model, Build. Environ. 24 (1989) 85–97, https://doi.org/10.1016/0360-1323(89)90019-X.
[19] F.R. Carrié, A. Mélois, Modelling building airtightness pressurisation tests with periodic wind and sharp-edged openings, Energy Build. 208 (2020), https://doi.org/10.1016/j.enbuild.2019.109642.
[20] M. Mahmoodzadeh, V. Gretka, S. Wong, T. Froese, P. Mukhopadhyaya, Evaluating patterns of building envelope air leakage with infrared thermography, Energies 13 (2020), https://doi.org/10.3390/en13143545 (Basel).
[21] E. Barreira, R.M.S.F. Almeida, M. Moreira, An infrared thermography passive approach to assess the effect of leakage points in buildings, Energy Build. 140 (2017) 224–235, https://doi.org/10.1016/j.enbuild.2017.02.009.
[22] N.P. Avdelidis, T.K. Kauppinen, Thermography as a tool for building applications and diagnostics, in: V.P. Vavilov, D.D. Burleigh (Eds.), Thermosense XXX, SPIE, 2008, p. 69390U, https://doi.org/10.1117/12.776463.
[23] B. Kölsch, J. Pernpeintner, B. Schiricke, E. Lüpfert, Air leakage detection in building façades by combining lock-in thermography with blower excitation, Int. J. Vent. 22 (2023) 357–365, https://doi.org/10.1080/14733315.2023.2198791.
[24] N. Hurel, M. Woloszyn, M. Pailha, B. Moujalled, Assessing the performance of infrared thermography and PIV methods to identify and characterize the air inlets and outlets in wall assemblies, J. Build. Eng. 95 (2024) 110308, https://doi.org/10.1016/J.JOBE.2024.110308.
[25] W. Liu, X. Zhao, Q. Chen, A novel method for measuring air infiltration rate in buildings, Energy Build. 168 (2018) 309–318, https://doi.org/10.1016/j.enbuild.2018.03.035.
[26] A. Royuela-del-Val, M.Á. Padilla-Marcos, A. Meiss, P. Casaseca-de-la-Higuera, J. Feijó-Muñoz, Air infiltration monitoring using thermography and neural networks, Energy Build. 191 (2019) 187–199, https://doi.org/10.1016/J.ENBUILD.2019.03.019.